



Published in final edited form as:

Retina. 2018 January ; 38(1): 29–38. doi:10.1097/IAE.0000000000001504.

Dynamism of dot subretinal drusenoid deposits in age-related macular degeneration demonstrated with adaptive optics imaging

Yuhua Zhang, PhD^{1,*}, Xiaolin Wang, MS¹, Pooja Godara, MD¹, Tianjiao Zhang, BS², Mark E. Clark, BS¹, C. Douglas Witherspoon, MD¹, Richard F. Spaide, MD³, Cynthia Owsley, PhD¹, and Christine A. Curcio, PhD¹

¹ Department of Ophthalmology, University of Alabama at Birmingham School of Medicine, Birmingham, Alabama

² Department of Bioengineering, University of California, Berkeley, California

³ Vitreous-Retina-Macula Consultants of New York, New York

Abstract

Purpose—To investigate the natural history of dot subretinal drusenoid deposits (SDD) in age-related macular degeneration (AMD), using high-resolution adaptive optics scanning laser ophthalmoscopy (AOSLO).

Methods—Six eyes of 4 patients with intermediate AMD were studied at baseline and 1 year later. Individual dot SDD within the central 30° retina were examined with AOSLO and optical coherence tomography.

Results—A total of 269 solitary SDD were identified at baseline. Over 12.25 ± 1.18 months, all 35 stage 1 SDD progressed to advanced stages. Eighteen (60%) stage 2 lesions progressed to stage 3 and 12 (40%) remained at stage 2. Of 204 stage 3 SDD, 12 (6.4%) disappeared and the rest remained. Twelve new SDD were identified, including 6 (50%) at stage 1, 2 (16.7%) at stage 2, and 4 (33.3%) at stage 3. The mean percentage of retina affected by dot SDD, measured by the AOSLO, increased in 5/6 eyes (from 2.31% to 5.08% in the most changed eye) and decreased slightly in 1/6 eye (from 10.67% to 10.54%). Dynamism, the absolute value of the areas affected by new and regressed lesions, ranged from 0.7% to 9.3%.

Conclusions—AOSLO reveals that dot SDD, like drusen, are dynamic.

*Correspondence and requests for reprints: Yuhua Zhang, PhD, Department of Ophthalmology, University of Alabama at Birmingham School of Medicine, Volker Hall 390C, 1670 University Boulevard, Birmingham, AL 35294. Phone: 205-996-8663, Fax: 205-934-3425, zhanghua@uab.edu.

Meeting Presentation: A part of this work was presented at the ARVO annual meeting held in Orlando, FL, May 6, 2014.

Financial Disclosures: No financial disclosures for Y Zhang, X Wang, P Godara, T Zhang, M E Clark, C D Witherspoon, C Owsley, and C A Curcio. R F Spaide receives consultant and royalty payment from Topcon Inc., Tokyo, Japan, Bausch and Lomb, Rochester, New York, USA.

List of Supplemental Digital Content

1. How plane of focus in adaptive optics scanning laser ophthalmoscopy (AOSLO) influences visibility of photoreceptors and subretinal drusenoid deposits (SDD), and thus accuracy of quantification
2. Figures 1-3 in main text rendered with an alternate labelling scheme not using color indicators

Keywords

age-related macular degeneration; subretinal drusenoid deposits; retina; adaptive optics scanning laser ophthalmoscopy; multimodal imaging; photoreceptors

INTRODUCTION

Subretinal drusenoid deposits (SDD) are extracellular lesions found between the photoreceptors and retinal pigment epithelium (RPE) layer.^{1, 2} These lesions clinically manifest as pseudodrusen,²⁻⁴ an entity first described by Mimoun et al. as a distinctive yellowish pattern “visible en lumière bleue” (visible in blue light) in many eyes with age-related macular degeneration (AMD).⁵ Pseudodrusen are highly associated with progression to neovascularization⁶ and geographic atrophy (GA),⁷⁻¹² two late stages of AMD. Recently Spaide described outer retinal atrophy, a severe photoreceptor degeneration in eyes with regressed SDD, suggested that this entity was a third form of late AMD.¹³ Compared to drusen, the hallmark extracellular lesion of AMD, SDD accumulate in a distinct layer of the outer retina,^{2, 3, 14} appear with different retinal topography,^{3, 15} and have similar proteins but different cholesterol forms.^{1, 16} The biogenesis and pathogenic significance of SDD in AMD pathophysiology are currently under intensive study by numerous investigators. Further, it is reasonable to expect that changes in the overall SDD population will be correlated to visual function of an eye with SDD.

Determining why and how SDD are linked to late stage AMD and how they impact vision would be assisted by an accurate natural history. SDD progression has been assessed at the eye level using standard clinical imaging modalities,^{9-11, 17-20} including infrared scanning laser ophthalmoscopy (SLO), autofluorescence, and spectral domain optical coherence tomography (SD-OCT). With SD-OCT, individual SDD lesions were classified into 3 stages by Zweifel et al.³ Querques et al suggested a fourth stage, of regression.¹⁷ There are challenges to assessing SDD regression accurately. It is difficult to precisely align OCT scans at the same location of the same lesion across different imaging sessions.²¹ SDD regression may involve several steps that are not currently defined. Since the original description of stages in SD-OCT,³ SDD morphologies of dot, ribbon (or reticular), and confluent have been clearly demonstrated in en face imaging.²²⁻²⁴ These forms appear to have their own progression sequences, with dot proceeding preferentially to neovascularization and confluent proceeding preferentially to geographic atrophy.²³ Precise observation of individual SDD may be informative about how these population changes arise.

Previously, we demonstrated that adaptive optics scanning laser ophthalmoscopy (AOSLO) can disclose SDD microstructure with unprecedented resolution and fidelity.^{25, 26} The purpose of our current study is to assess SDD dynamism at the level of individual dot lesions using AOSLO over a 12 month period. Conducting in vivo microscopy of SDD progression in this manner will allow us to answer important questions: do dot SDD progress directly along stages 1-2-3? Do lesions disappear? By studying every dot SDD within a region of

interest (ROI), we can precisely assess their impact on overlying neurosensory retina during different phases of the lesion lifecycle.

METHODS

The study followed the tenets of the Declaration of Helsinki, complied with the Health Insurance Portability and Accountability Act of 1996, and was approved by the Institutional Review Board at the University of Alabama at Birmingham. Written informed consent was obtained from participants after the nature and possible consequences of the study were explained.

Patients

Study patients were a subgroup from an earlier study of SDD microstructure.²⁶ Patients previously diagnosed with AMD were recruited from the clinical research registry of the Department of Ophthalmology of the University of Alabama at Birmingham and through the Retina Service. AMD presence and severity were determined by masked grading of fundus photos using the Age-Related Eye Disease Study (AREDS) severity scale.²⁷ Stereoscopic color digital 30° fundus photographs were taken with a FF450 Plus fundus camera (Carl Zeiss Meditec, Dublin, CA) after pupil dilation. Disease severity ranged from early to intermediate (AREDS grade 2-8). Exclusion criteria at enrollment were diabetes, history of retinal vascular occlusions, and any signs or history of hereditary retinal dystrophy. If patients developed any of the following conditions after enrollment, they were also excluded from the analyses reported here: neovascularization or any other retinal disease in the study eye such as retinal vascular (diabetic retinopathy, retinal vein occlusion) or vitreoretinal (vitreomacular traction syndrome, epiretinal membrane) disease. Subjects were also excluded for reasons that might potentially prevent successful imaging, such as poor fixation, significant media opacity, irregular pupil shape, poor dilation, or refractive error beyond ± 6 D spherical and ± 3 D cylinder. All participants underwent best-corrected visual acuity (BCVA) measurement by the Electronic Visual Acuity (EVA) protocol.²⁸

Timeline and study protocol

Baseline imaging was conducted between February 2012 and January 2013. Follow-up imaging using the same procedures was performed between April 2013 and August 2013. Imaging procedures were detailed previously²⁶ and are briefly summarized here. Due to some patients moving away from the area and development of other conditions (e.g., neovascularization), only some patients studied at baseline returned for follow-up study.

High-resolution AOSLO image acquisition and process

The AOSLO is a new generation research system equipped with a custom high-speed Shack-Hartmann wavefront sensor and a high-speed deformable mirror (Hi-Speed DM97-15, ALPAO SAS, France) with 97 actuators with stroke up to 30 μm that provide improved correction ability for wavefront distortion.^{25, 26, 29, 30} It uses a low coherence light source (Broadlighter S840-HP, Superlum, Russia) to mitigate light interference artifact thereby producing high fidelity retinal images.³¹ The AOSLO acquires retinal images with a field of view of $1.2^\circ \times 1.2^\circ$ inside the eye at a frame rate of 15 Hz. Before imaging, pupils were

dilated with 1.0% tropicamide and 2.5% phenylephrine hydrochloride. AOSLO videos were recorded continuously across an area about $20^{\circ} \times 20^{\circ}$. Registered images were averaged to enhance signal-to-noise ratio. Images of different retinal locations were manually aligned on a cell-to-cell basis to create a montage using professional image processing software (Photoshop, Adobe Systems Inc., Mountain View, CA). AOSLO image pixel size was computed from an image of a precisely calibrated dot grid placed at the retinal plane of a model eye.

Multimodal imaging and registration

Color fundus photographs, en face near-infrared reflectance (NIR) ($\lambda = 830$ nm), red-free ($\lambda = 560$ nm), and autofluorescence (excitation, 488 nm; emission, > 600 nm) images were acquired with the confocal SLO of the Spectralis (Heidelberg Engineering, Carlsbad, CA). All images were acquired with a 30° field of view. Retinal cross-sections were imaged with the Spectralis SD-OCT ($\lambda = 870$ nm; scan depth, 1.9 mm; axial resolution, $3.5 \mu\text{m}$ per pixel in tissue; lateral resolution, $14 \mu\text{m}$ per pixel in tissue). In each study eye, 97 B-scans were acquired across a $15^{\circ} \times 10^{\circ}$ area of the central macula to create a volume at the baseline study. At follow-up, the scan volume was extended to 194 B-scans across the central $20^{\circ} \times 20^{\circ}$ macula. We use nomenclature of Staurengi and associates for SD-OCT bands.³² Color fundus photographs and en face NIR, red-free, and autofluorescence images were registered manually by use of retinal vessels and capillaries as fiduciary landmarks. Color fundus photographs and SLO NIR images were then magnified and registered with the AOSLO montage by use of retinal vessels and capillaries as landmarks. For Figures 1-3, alternate labelling schemes not using color are available as Supplemental Figures 1-3.

SDD identification and classification

SDD identified by presence in at least 2 *en face* imaging modalities and in SD-OCT at baseline were also examined at follow-up. Each lesion was scored with the 3-stage grading system of Zweifel et al.³ In all patients both dot and ‘ribbon’ SDD were discerned, and for analysis, we chose to follow the progression of ‘dots’ for comparability with previous studies^{17, 21, 33} and also because our imaging instrument did not reveal ribbon SDD distinctly.

Quantifying SDD-affected area in the central 30° of the macula imaged by AOSLO and NIR reflectance

At baseline and follow-up, multiple regions of interest (ROI) containing SDD representing local lesion distribution were selected in AOSLO images. In each ROI, the hyporeflective area of retina associated with each individual SDD²⁶ was delineated manually using the Polygon Selections tool and summed using the “Analyze Particles” tool of ImageJ (version 1.50a; <http://rsbweb.nih.gov/ij/>; National Institutes of Health, Bethesda, MD). For stage 1 and 2 lesions, the affected retinal area was hyporeflective. For stage 3 lesions the affected area included a hyporeflective annulus plus the hyperreflective SDD in the center.

Because most dot SDD are conical, en face cross-sectional areas of individual lesions could vary with the level of AOSLO focus. Therefore, SDD areas were measured only at a focal plane where surrounding cone inner segments were apparent (see **Figure CD**,

Supplemental Digital Content 1). Because AOSLO has axial resolution of 70 μm , images are formed by aggregate light reflected from a volume of dimensions 2.8 $\mu\text{m} \times 2.8 \mu\text{m} \times 70 \mu\text{m}$ (the lateral resolution of AOSLO is 2.8 μm). When defocus in either direction from the plane of best photoreceptor visibility exceeds axial resolution, cells are not visible (see **Figure AB, EF, Supplemental Digital Content 1**).

In focused images, we measured the following:

- 1) Sizes of individual SDD affected retina areas are reported in units of equivalent diameter d_i (μm), which were calculated by

$$d_i = 2\sqrt{s_i/\pi},$$

where s_i is the retinal area affected by an individual lesion, and π is the constant ratio of a circle's circumference to its diameter. To assist manual delineation, the borders of hyporeflective retina associated with each individual SDD were identified and enhanced in 2 standardized steps (Photoshop, Adobe Systems Inc., Mountain View, CA). The image was first filtered (Filter > Blur > Gaussian Blur. 'Radius' = 3 pixels), then sharpened (Filter > Sharpen > Smart Sharpen. 'Amount' = 180%, 'Radius' = 64 pixels). Parameter settings were determined by 2 experienced observers (authors YZ and XW) in preliminary studies.

- 2) For each ROI, the mean percentage of ROI affected by SDD is reported. To avoid bias, multiple ROIs sampled from different retinal areas in the AOSLO montage were pooled to calculate a mean percentage of ROI affected by SDD.

- 3) The area containing SDD in the central 30° (in units of mm^2) was outlined (ImageJ, Polygon tool), after the method of Steinberg and associates.¹⁸

- 4) The burden of SDD (in units of mm^2) was the product of the percentage of the ROI affected by SDD and the area containing SDD in the central 30° (calculations #2 and 3).

- 5) To assess SDD dynamism, we computed for each eye's pooled ROI (see #2 above), the aggregate percentage of ROI affected by stable, new, and regressed SDD, per the method of Smith and associates for drusen visualized by color fundus photography.³⁴ Dynamism is the absolute value of percent of new plus regressed lesions. Net change from baseline to follow-up is calculated as (% stable + new – regressed).

RESULTS

Four patients with intermediate stage AMD (AREDS 5-7), all white of European descent, met enrollment criteria. Six eyes were studied at baseline and then approximately 12 months later (mean \pm standard deviation: 12.25 \pm 1.18 months).

AOSLO disclosed the dynamism of SDD progression and regression (**Figure 1**). Lesions can appear (green arrows), expand (yellow arrows), shrink (red arrowheads), and disappear (yellow and magenta arrowheads). Corresponding changes are also visible in cross-sectional

SD-OCT. **Figure 2** shows that individual lesions at the same stage are distinct enough to be readily followed. **Figure 3** demonstrates a monotonic progression from stage 2 to 3 via 2 different B-scans through each lesion. It also confirms how the size of individual lesions revealed by SD-OCT is highly dependent on the position of the scan, as previously stated.¹⁹

A total of 269 solitary SDD identified at baseline were also seen at follow-up (**Figure 4**). Of these, 35 (13.0%) were classified as stage 1, 30 (11.2%) as stage 2, and 204 (75.8%) as stage 3. Over 12 months, of the 35 lesions that were stage 1 at baseline, 3 (8.6%) progressed to stage 2, and 32 (91.4%) progressed to stage 3. Of the 30 lesions that were stage 2 at baseline, 18 (60.0%) progressed to stage 3, and 12 (40.0%) remained at stage 2. For the 204 lesions that were stage 3 at baseline, 13 (6.4%) disappeared, and 191 (93.6%) remained at stage 3. Of the 13 lesions that disappeared, 6 were associated with focal hyperreflectivity in the outer nuclear layer, as described by Querques et al.¹⁷ To contextualize this intraretinal hyperreflectivity, we randomly chose 50 stage 3 SDD that did not disappear and found that 15 of these lesions also were associated with focal hyperreflectivity. Finally, 12 newly developed SDD were identified, of which 6 (50%) were stage 1, 2 (16.7%) were stage 2, and 4 (33.3%) were stage 3.

Mean equivalent diameters of SDD-affected retinal areas at baseline and follow-up (**Table 1**) increased over the follow-up period. Mean values tend to mask time-dependent changes of individual lesions, and it was noted that lesions remaining at the same stage could still change size. For 12 SDD remaining at stage 2, 9 (75%) enlarged, and 3 (25%) shrank. For 191 SDD remaining at stage 3, 139 (73%) enlarged, and 52 (27%) shrank.

Figure 5, top row, shows that in 5/6 eyes, the mean percentage of ROI affected by SDD increased (range, baseline to follow-up: 7.5%-9.0%, a 20.0% increase; 14.4%-20.7%, a 43.8% increase). In one eye, the percentage of ROI affected by SDD decreased slightly (10.7%-10.5%). **Figure 5**, bottom row, accordingly shows that in 5/6 eyes, lesion burden over the central 30° increased (range, baseline to follow-up: 5.24-6.72 mm², a 28.3% increase; 0.36-1.45 mm², a 306.8% increase). In one eye, lesion burden decreased 1% (7.88-7.80 mm²). In 5 eyes the retinal area containing SDD extended beyond the 30° imaged by NIR. Thus, lesion burden assessed within the central 30° is an underestimate of the true burden.

Table 2 shows for each eye the percentage of ROI affected by SDD that were stable, new, or regressed, and the results for absolute net change are consistent with **Figure 5**. Dynamism is a measure of overall disease activity, defined as the sum of areas affected by new and regressed lesions, ranged from 0.7% in eye 2 to 9.3% in eye 1. Eye 4 had a slight net loss over the observation period, yet had nearly equal growth and regression.

DISCUSSION

In this study, we demonstrated progression of individual SDD over a period of approximately 12 months using high resolution AOSLO. SDD progressed from early to advanced stages, and no SDD at stage 1 or 2 at baseline disappeared, supporting an evolution implied by the Zweifel 3-stage system.³ We confirmed that some stage 3 SDD

indeed disappeared, as suggested by Querques and colleagues who observed in 48 patients followed 24 months a fading of subretinal material accompanied by EZ disruption and loss.¹⁷ Longitudinal follow-up of individual lesions over time indicates that SDD are dynamic, as are drusen. If populations of SDD regress, with loss of architecture of the superjacent retina, the net result is outer retinal atrophy.¹³

Our evidence for SDD disappearance is strong, because for each individual lesion seen in AOSLO, the subretinal location and stage was corroborated in SD-OCT. Our findings are not necessarily inconsistent with those of Steinberg et al,²¹ who did not observe SDD disappearance in 18 eyes of 12 patients in shorter periods (2-10 months), even with dense SD-OCT volumes (11 μm spacing). Steinberg suggested that misaligned B-scans across imaging sessions could cause a false impression of lesion disappearance if they transected edges rather than centers of lesions at follow-up, which we demonstrate here in correlated AOSLO and SD-OCT (Figure 3). Pixel-to-pixel correlation in the Spectralis OCT-SLO is now known to have a co-localization error of $42.2 \pm 32.4 \mu\text{m}^{35}$ due to optical resolution (14 μm lateral), image digitation (pixel size: 6-11 $\mu\text{m}/\text{pixel}$), signal-to-noise ratio, and within-frame image distortion³⁶ introduced by eye movement.³⁷ AOSLO provides lateral resolution of 2.8 μm which is $\sim 1/10$ th of the diameter of the smallest SDD detected.²⁶ Using photoreceptors mosaic as an en face reference (see **Figure, Supplemental Digital Content 1**), we could observe stage-specific structure and dimension of individual lesions²⁶ over time more accurately than had we used B-scan alignment alone. Thus even with a follow-up period not that much longer than Steinberg et al,²¹ we were able to confirm SDD disappearance.¹⁷

A concept learned from drusen and applicable to SDD is that extracellular lesions are dynamic with stages of development, progression, and regression, involving participation of neighboring cells. Drusen undergo growth followed by collapse, as described in histopathology^{38, 39} and recently quantified with OCT technologies, some automated.⁴⁰⁻⁴⁴ One model of druse growth involves retention of RPE-secreted material including lipoproteins by aging Bruch's membrane.⁴⁵ The cells and secreted factors (e.g., metalloproteinases, lipases) responsible for druse removal are not established. Macrophages are widely thought to clear drusen^{39, 46} yet direct evidence on this point is scant. On the other hand, Müller cell gliosis is prominent in atrophic areas,^{47, 48} and processes of presumed Müller cells appear to break up basal laminar deposit persisting after the death of overlying RPE.⁴⁹ Further, microglia invade outer retina in areas of photoreceptor loss^{50, 51} and in eyes with drusen cleared by experimental nanosecond laser treatment.⁵²

SDD dynamism is a balance of production and clearance of molecules secreted by neighboring cells involved in lipid recycling,² retinoid processing,²² and other activities. Querques and coworkers reported punctate hyperreflectivity 'flying' into the inner retina over disappeared lesions (Fig 6 of ¹⁷), speculating that lesion material could eventually migrate within the inner retinal layers.¹⁷ By histology Rudolf and associates showed gaps in the outer nuclear layer atop individual lesions,¹ and Greferath and colleagues demonstrated vitronectin-immunoreactive SDD material within such gaps.⁴ These latter authors further reported that Müller cells were focally reactive over clinically documented stage 1-2 lesions, and Iba-1-immunoreactive microglia in the subretinal space associated with the apices of

stage 3 lesions.⁴ These observations are consistent with removal of SDD material by cells in the retina; whether this material is also associated with hyperreflectivity is currently unknown. Our current data cannot address whether reflective material in ONL is SDD and whether it is specifically associated with lesion disappearance. Data from more lesions at a longer follow-up, ideally with histopathologic correlation, are required to determine the nature of this material.

Previous measures of SDD load in individual eyes included the area affected and number of lesions.^{21, 33} In our limited sample of eyes, as much as 20% of any one retinal location could be affected, and this percentage could go up or down in follow-up. As reported for drusen,³⁴ an eye could exhibit little net change yet have simultaneous growth and regression suggesting very active disease (eye 4 in Table 2). SDD's subretinal location suggests a direct effect on surrounding photoreceptors in addition to impaired transport to and from the choroid.² In SDD-bearing areas of eyes with intermediate AMD, photopic and mesopic sensitivity is reduced, as tested by microperimetry.⁵³⁻⁵⁶ Further, dark adaptation is so impaired in such eyes⁵⁴ that involvement of a widespread retinal or RPE dysfunction beyond the directly affected photoreceptors is highly likely. Visual sensitivity is very poor when SDD involute and the outer retina collapses. Our SDD metrics may thus have their greatest value in assessing the functional impact of SDD in early AMD; more research on this point is needed.

Previously used in clinical trials for counting cone photoreceptors,⁵⁷ AOSLO was used herein to measure percentage of outer retina affected by SDD and the burden and dynamism of lesions in the aggregate. These measures may be used as clinical endpoints for evaluating agents designed to reduce SDD, when these become available. Because we could characterize SDD progression and regression at the level of individual lesions within a period of just over a year, use of AOSLO could effectively shorten the length and reduce the cost of proof-of-concept clinical trials, as suggested for measuring aggregate druse volume.⁵⁸

A strength of our study is the stage determination by both en face and cross-sectional imaging for each of many individual SDD lesions. Limitations are the short follow-up period, the small number of eyes, and the attention to dot lesions over other SDD subtypes. Although the percentage of retina affected by individual SDD was assessed in multiple ROIs, AOSLO images were acquired within the central 20°, so we likely underestimated lesion load. Potential bias in the selection of AOSLO ROIs can be reduced in future studies using systematic sampling. Our ongoing and future studies involve a longer follow-up assessment of photoreceptors status, including use of directional OCT⁵⁹ and development of software for automated calculation of SDD burden. Nevertheless, current data motivate histological studies of SDD clearance as well as *in vivo* studies designed to derive a quantitative relationship between lesion burden and photoreceptor function, especially in early AMD. In conclusion, we improved our knowledge of the SDD dynamism with multimodal high-resolution imaging and deepened our understanding of SDD's role in AMD pathobiology.

Supplementary Material

Refer to Web version on PubMed Central for supplementary material.

Acknowledgments

Funding/Support: This project was supported in part by EY021903, EY024378, AG04212, and EY06109 and institutional support from Research to Prevent Blindness, EyeSight Foundation of Alabama, Buck Trust of Alabama, the Dorsett Davis Discovery Fund.

REFERENCES

1. Rudolf M, Malek G, Messinger JD, Clark ME, Wang L, Curcio CA. Sub-retinal drusenoid deposits in human retina: organization and composition. *Exp Eye Res.* 2008; 87:402–8. [PubMed: 18721807]
2. Curcio CA, Messinger JD, Sloan KR, McGwin G, Medeiros NE, Spaide RF. Subretinal drusenoid deposits in non-neovascular age-related macular degeneration: morphology, prevalence, topography, and biogenesis model. *Retina.* 2013; 33:265–76. [PubMed: 23266879]
3. Zweifel SA, Spaide RF, Curcio CA, Malek G, Imamura Y. Reticular pseudodrusen are subretinal drusenoid deposits. *Ophthalmology.* 2010; 117:303–12. e1. [PubMed: 19815280]
4. Greferath U, Guymer RH, Vessey KA, Brassington K, Fletcher EL. Correlation of Histologic Features with In Vivo Imaging of Reticular Pseudodrusen. *Ophthalmology.* 2016; 123:1320–31. [PubMed: 27039021]
5. Mimoun G, Soubrane G, Coscas G. Le drusen maculaires. *J Fr Ophthalmol.* 1990; 13:511–30.
6. Cohen SY, Dubois L, Tadayoni R, Delahaye-Mazza C, Debibie C, Quentel G. Prevalence of reticular pseudodrusen in age-related macular degeneration with newly diagnosed choroidal neovascularisation. *Br J Ophthalmol.* 2007; 91:354–9. [PubMed: 16973663]
7. Klein R, Meuer SM, Knudtson MD, Iyengar SK, Klein BE. The epidemiology of retinal reticular drusen. *Am J Ophthalmol.* 2008; 145:317–326. [PubMed: 18045568]
8. Schmitz-Valckenberg S, Alten F, Steinberg JS, et al. Reticular drusen associated with geographic atrophy in age-related macular degeneration. *Invest Ophthalmol Vis Sci.* 2011; 52:5009–15. [PubMed: 21498612]
9. Sarks J, Arnold J, Ho IV, Sarks S, Killingsworth M. Evolution of reticular pseudodrusen. *Br J Ophthalmol.* 2011; 95:979–85. [PubMed: 21109695]
10. Xu L, Blonska AM, Pumariega NM, et al. Reticular macular disease is associated with multilobular geographic atrophy in age-related macular degeneration. *Retina.* 2013; 33:1850–62. [PubMed: 23632954]
11. Marsiglia M, Boddu S, Bearely S, et al. Association between geographic atrophy progression and reticular pseudodrusen in eyes with dry age-related macular degeneration. *Invest Ophthalmol Vis Sci.* 2013; 54:7362–9. [PubMed: 24114542]
12. Finger RP, Wu Z, Luu CD, et al. Reticular pseudodrusen: a risk factor for geographic atrophy in fellow eyes of individuals with unilateral choroidal neovascularization. *Ophthalmology.* 2014; 121:1252–6. [PubMed: 24518615]
13. Spaide RF. Outer retinal atrophy after regression of subretinal drusenoid deposits as a newly recognized form of late age-related macular degeneration. *Retina.* 2013; 33:1800–8. [PubMed: 23764969]
14. Spaide RF, Curcio CA, Zweifel SA. Drusen, an old but new frontier. *Retina.* 2010; 30:1163–5. [PubMed: 20827136]
15. Spaide RF, Curcio CA. Drusen characterization with multimodal imaging. *Retina.* 2010; 30:1441–54. [PubMed: 20924263]
16. Oak AS, Messinger JD, Curcio CA. Subretinal drusenoid deposits: further characterization by lipid histochemistry. *Retina.* 2014; 34:825–6. [PubMed: 24589874]

17. Querques G, Canoui-Poitaine F, Coscas F, et al. Analysis of progression of reticular pseudodrusen by spectral domain-optical coherence tomography. *Invest Ophthalmol Vis Sci.* 2012; 53:1264–70. [PubMed: 22266524]
18. Steinberg JS, Auge J, Jaffe GJ, et al. Longitudinal analysis of reticular drusen associated with geographic atrophy in age-related macular degeneration. *Invest Ophthalmol Vis Sci.* 2013; 54:4054–60. [PubMed: 23633663]
19. S. SJSAJFMHFGS-V. Longitudinal Analysis of Reticular Drusen Associated with Age-Related Macular Degeneration Using Combined Confocal Scanning Laser Ophthalmoscopy and Spectral-Domain Optical Coherence Tomography Imaging. *Ophthalmologica.* 2015; 233:35–42. [PubMed: 25413846]
20. Steinberg JS, Gobel AP, Fleckenstein M, Holz FG, Schmitz-Valckenberg S. Reticular drusen in eyes with high-risk characteristics for progression to late-stage age-related macular degeneration. *Br J Ophthalmol.* 2015; 99:1289–94. [PubMed: 25795913]
21. Steinberg JS, Auge J, Fleckenstein M, Holz FG, Schmitz-Valckenberg S. Longitudinal analysis of reticular drusen associated with age-related macular degeneration using combined confocal scanning laser ophthalmoscopy and spectral-domain optical coherence tomography imaging. *Ophthalmologica.* 2015; 233:35–42. [PubMed: 25413846]
22. Suzuki M, Sato T, Spaide RF. Pseudodrusen subtypes as delineated by multimodal imaging of the fundus. *Am J Ophthalmol.* 2014; 157:1005–12. [PubMed: 24503406]
23. Zhou Q, Daniel E, Maguire MG, et al. Pseudodrusen and Incidence of Late Age-Related Macular Degeneration in Fellow Eyes in the Comparison of Age-Related Macular Degeneration Treatments Trials. *Ophthalmology.* 2016; 123:1530–40. [PubMed: 27040149]
24. Lee MY, Yoon J, Ham DI. Clinical features of reticular pseudodrusen according to the fundus distribution. *Br J Ophthalmol.* 2012; 96:1222–6. [PubMed: 22773089]
25. Meadway A, Wang X, Curcio CA, Zhang Y. Microstructure of subretinal drusenoid deposits revealed by adaptive optics imaging. *Biomed Opt Express.* 2014; 5:713–727. [PubMed: 24688808]
26. Zhang Y, Wang X, Rivero EB, et al. Photoreceptor perturbation around subretinal drusenoid deposits as revealed by adaptive optics scanning laser ophthalmoscopy. *Am J Ophthalmol.* 2014; 158:584–96. e1. [PubMed: 24907433]
27. Davis MD, Gangnon RE, Lee LY, et al. The Age-Related Eye Disease Study severity scale for age-related macular degeneration: AREDS Report No. 17. *Archives of ophthalmology.* 2005; 123:1484–98. [PubMed: 16286610]
28. Beck RW, Moke PS, Turpin AH, et al. A computerized method of visual acuity testing: adaptation of the early treatment of diabetic retinopathy study testing protocol. *Am J Ophthalmol.* 2003; 135:194–205. [PubMed: 12566024]
29. Meadway A, Girkin CA, Zhang Y. A dual-modal retinal imaging system with adaptive optics. *Opt Express.* 2013; 21:29792–807. [PubMed: 24514529]
30. Yu Y, Zhang T, Meadway A, Wang X, Zhang Y. High-speed adaptive optics for imaging of the living human eye. *Opt Express.* 2015; 23:23035–52. [PubMed: 26368408]
31. Putnam NM, Hammer DX, Zhang Y, Merino D, Roorda A. Modeling the foveal cone mosaic imaged with adaptive optics scanning laser ophthalmoscopy. *Opt Express.* 2010; 18:24902–16. [PubMed: 21164835]
32. Staurengi G, Sadda S, Chakravarthy U, Spaide RF. International Nomenclature for Optical Coherence Tomography P. Proposed lexicon for anatomic landmarks in normal posterior segment spectral-domain optical coherence tomography: the IN*OCT consensus. *Ophthalmology.* 2014; 121:1572–8. [PubMed: 24755005]
33. Alten F, Heiduschka P, Clemens CR, Eter N. Longitudinal structure/function analysis in reticular pseudodrusen. *Invest Ophthalmol Vis Sci.* 2014; 55:6073–81. [PubMed: 25146989]
34. Smith RT, Sohrab MA, Pumariega N, et al. Dynamic soft drusen remodelling in age-related macular degeneration. *Br J Ophthalmol.* 2010; 94:1618–23. [PubMed: 20530179]
35. Vongkulsiri S, Spaide RF. Colocalization error between the scanning laser ophthalmoscope infrared reflectance and optical coherence tomography images of the heidelberg spectralis. *Retina.* 2015; 6:1211–5. M. S.

36. Vogel CR, Arathorn DW, Roorda A, Parker A. Retinal motion estimation in adaptive optics scanning laser ophthalmoscopy. *Opt Express*. 2006; 14:487–97. [PubMed: 19503363]
37. Rolfs M. Microsaccades: small steps on a long way. *Vision research*. 2009; 49:2415–41. [PubMed: 19683016]
38. Gass JDM. Drusen and disciform macular detachment and degeneration. *Arch Ophthalmol*. 1973; 90:206–17. [PubMed: 4738143]
39. Sarks JP, Sarks SH, Killingsworth MC. Evolution of soft drusen in age-related macular degeneration. *Eye (London, England)*. 1994; 8:269–83. Pt 3.
40. Khanifar AA, Koreishi AF, Izatt JA, Toth CA. Drusen ultrastructure imaging with spectral domain optical coherence tomography in age-related macular degeneration. *Ophthalmology*. 2008; 115:1883–90. [PubMed: 18722666]
41. Yehoshua Z, Wang F, Rosenfeld PJ, Penha FM, Feuer WJ, Gregori G. Natural history of drusen morphology in age-related macular degeneration using spectral domain optical coherence tomography. *Ophthalmology*. 2011; 118:2434–41. [PubMed: 21724264]
42. de Sisternes L, Simon N, Tibshirani R, Leng T, Rubin DL. Quantitative SD-OCT imaging biomarkers as indicators of age-related macular degeneration progression. *Invest Ophthalmol Vis Sci*. 2014; 55:7093–103. [PubMed: 25301882]
43. Schlanitz FG, Baumann B, Kundi M, et al. Drusen volume development over time and its relevance to the course of age-related macular degeneration. *Br J Ophthalmol*. 2016 PMID 27044341.
44. Balaratnasingam C, Yannuzzi LA, Curcio CA, et al. Associations Between Retinal Pigment Epithelium and Drusen Volume Changes During the Lifecycle of Large Drusenoid Pigment Epithelial Detachments. *Invest Ophthalmol Vis Sci*. 2016; 57:5479–5489. [PubMed: 27760262]
45. Curcio CA, Johnson M, Huang JD, Rudolf M. Aging, age-related macular degeneration, and the response-to-retention of apolipoprotein B-containing lipoproteins. *Prog Retin Eye Res*. 2009; 28:393–422. [PubMed: 19698799]
46. Sarks JP, Sarks SH, Killingsworth MC. Evolution of geographic atrophy of the retinal pigment epithelium. *Eye (London, England)*. 1988; 2:552–77. Pt 5.
47. Guidry C, Medeiros NE, Curcio CA. Phenotypic variation of retinal pigment epithelium in age-related macular degeneration. *Invest Ophthalmol Vis Sci*. 2002; 43:267–73. [PubMed: 11773041]
48. Wu KH, Madigan MC, Billson FA, Penfold PL. Differential expression of GFAP in early v late AMD: a quantitative analysis. *Br J Ophthalmol*. 2003; 87:1159–66. [PubMed: 12928288]
49. Ooto S, Vongkulsiri S, Sato T, Suzuki M, Curcio CA, Spaide RF. Outer retinal corrugations in age-related macular degeneration. *JAMA Ophthalmol*. 2014; 132:806–13. [PubMed: 24801396]
50. Lad EM, Cousins SW, Van Arnam JS, Proia AD. Abundance of infiltrating CD163+ cells in the retina of postmortem eyes with dry and neovascular age-related macular degeneration. *Graefes Arch Clin Exp Ophthalmol*. 2015; 253:1941–5. [PubMed: 26148801]
51. Zhao L, Zabel MK, Wang X, et al. Microglial phagocytosis of living photoreceptors contributes to inherited retinal degeneration. *EMBO Mol Med*. 2015; 7:1179–97. [PubMed: 26139610]
52. Jobling AI, Guymer RH, Vessey KA, et al. Nanosecond laser therapy reverses pathologic and molecular changes in age-related macular degeneration without retinal damage. *FASEB J*. 2015; 29:696–710. [PubMed: 25392267]
53. Querques G, Massamba N, Srour M, Boulanger E, Georges A, Souied EH. Impact of reticular pseudodrusen on macular function. *Retina*. 2014; 34:321–9. [PubMed: 23842105]
54. Flamendorf J, Agron E, Wong WT, et al. Impairments in Dark Adaptation Are Associated with Age-Related Macular Degeneration Severity and Reticular Pseudodrusen. *Ophthalmology*. 2015; 122:2053–62. [PubMed: 26253372]
55. Steinberg JS, Fitzke FW, Fimmers R, Fleckenstein M, Holz FG, Schmitz-Valckenberg S. Scotopic and Photopic Microperimetry in Patients With Reticular Drusen and Age-Related Macular Degeneration. *JAMA Ophthalmol*. 2015; 133:690–7. [PubMed: 25811917]
56. Steinberg JS, Sassmannshausen M, Fleckenstein M, et al. Correlation of partial outer retinal thickness with scotopic and mesopic fundus-controlled perimetry in patients with reticular drusen. *Am J Ophthalmol*. 2016

57. Talcott KE, Ratnam K, Sundquist SM, et al. Longitudinal study of cone photoreceptors during retinal degeneration and in response to ciliary neurotrophic factor treatment. *Invest Ophthalmol Vis Sci.* 2011; 52:2219–26. [PubMed: 21087953]
58. Schaal KB, Rosenfeld PJ, Gregori G, Yehoshua Z, Feuer WJ. Anatomic Clinical Trial Endpoints for Nonexudative Age-Related Macular Degeneration. *Ophthalmology.* 2016; 123:1060–79. [PubMed: 26952592]
59. Lujan BJ, Roorda A, Knighton RW, Carroll J. Revealing Henle's fiber layer using spectral domain optical coherence tomography. *Invest Ophthalmol Vis Sci.* 2011; 52:1486–92. [PubMed: 21071737]
60. Xu X, Liu X, Wang X, et al. Retinal pigment epithelium degeneration associated with subretinal drusenoid deposits in age-related macular degeneration. *Am J Ophthalmol.* 2016 in revision.

Summary statement

We used multimodal retinal imaging featuring adaptive optics scanning laser ophthalmoscopy to assess the natural history of subretinal drusenoid deposits (SDD) at the level of individual lesions. Our data demonstrate that SDD, like drusen, are dynamic and exhibit both growth and regression.

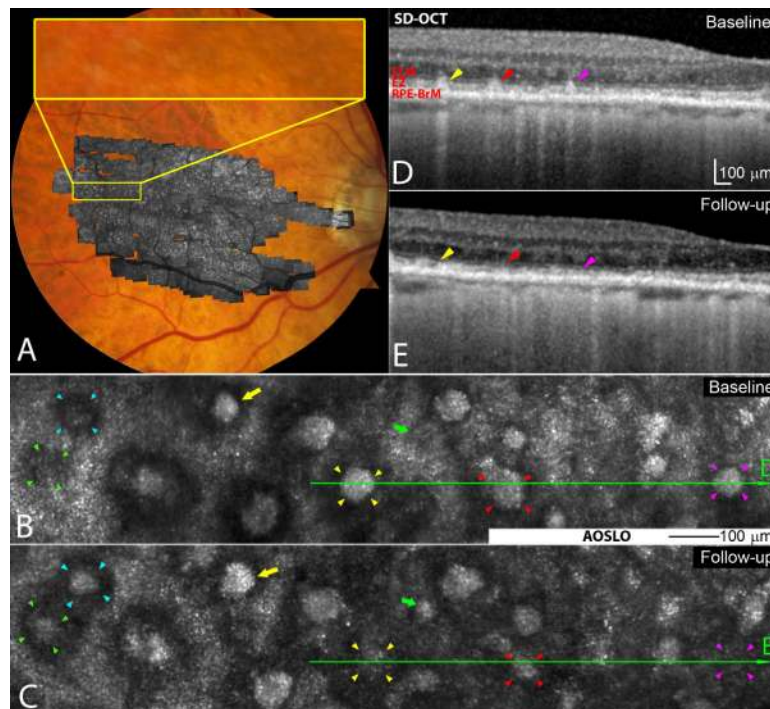


Figure 1.

Subretinal drusenoid deposit (SDD) dynamism imaged by multimodal imaging. **A.** Adaptive optics scanning laser ophthalmoscopy (AOSLO) montage (in grey scale) is overlaid on the digital fundus photograph of 30° field of view. **B & C.** AOSLO images of the retina area shown in the yellow box in (A) taken at baseline and 2nd visit (14 months later), revealing SDD progression. A stage 1 lesion progressed to stage 3 (green arrowheads 5), and a stage 2 lesion progressed to stage 3 (aqua). Stage 3 lesions may expand (yellow arrows), shrink (red arrowheads), and disappear (yellow and magenta arrowheads). New lesions can develop (green arrows). **D & E.** Stage-specific changes in SDD appearance are also clear in corresponding spectral domain optical coherence tomography (SD-OCT) B-scans, as indicated by green lines with arrows in (B) and (C). Stripes of hypertransmission into the choroid indicating retinal pigment epithelium degeneration are apparent,¹⁵ as will be described in a separate report.⁶⁰ The subject is an 84-year-old (at the baseline study) woman (white non-Hispanic) with non-neovascular AMD (Age-Related Eye Disease Study grade 7, best-corrected visual acuity 20/20). An alternate labelling scheme not using color is available as Supplemental Digital Content 2. ELM: external limiting membrane. EZ: ellipsoid zone. RPE-BrM: retinal pigment epithelium-Bruch's membrane.

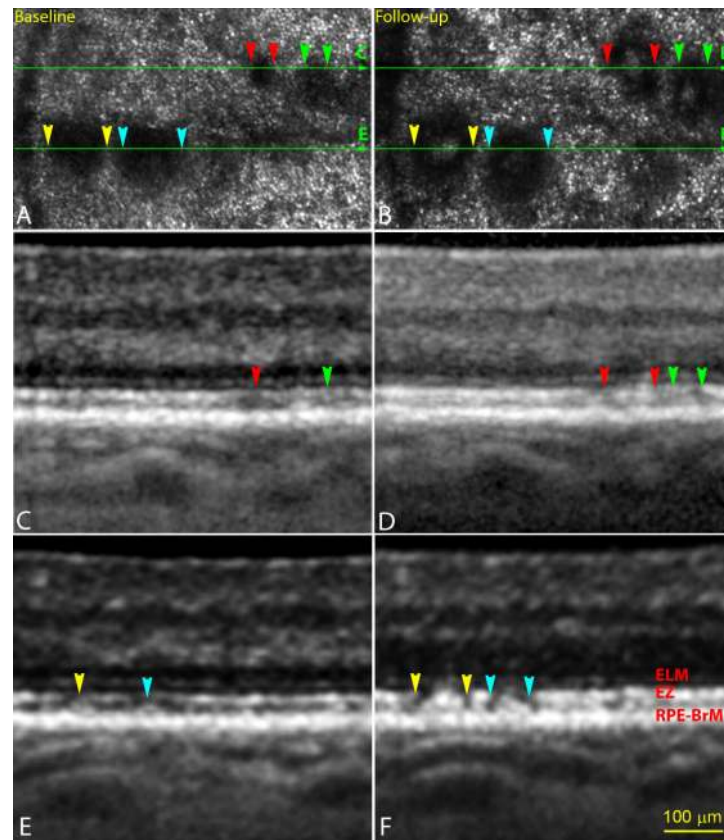


Figure 2.

Individuality of subretinal drusenoid deposit (SDD) progression. **A & B.** Adaptive optics scanning laser ophthalmoscopy (AOSLO) of the same retinal area taken at baseline and 2nd visit (14 months later). **C & D.** Spectral domain optical coherence tomography (SD-OCT) B-scan of the retina as indicated by the green arrow lines in (A) and (B). A stage-1 SDD (red arrowheads) and a stage-2 SDD (green arrowheads) at baseline progressed to stage-3. Dark gaps appeared in ellipsoid zone (EZ) band beside the SDD (panel D). **E & F.** SD-OCT B-scan of the retina as indicated by the green arrow lines in (A) and (B). Two stage-2 lesions (yellow and aqua arrowheads) at baseline progressed to stage-3. One lesion (yellow) was slightly larger than the other (aqua) at both baseline and follow-up, as apparent by both imaging modalities. Dark gaps clearly appeared in EZ band beside the SDD (panel F). The subject (AMD-041) is a 73-year-old (at baseline) man (white non-Hispanic) with non-neovascular age-related macular degeneration (Age-Related Eye Disease Study grade 6, best-corrected visual acuity 20/25). An alternate labelling scheme not using color is available as Supplemental Digital Content 3. ELM: external limiting membrane. RPE-BrM: retinal pigment epithelium-Bruch's membrane.

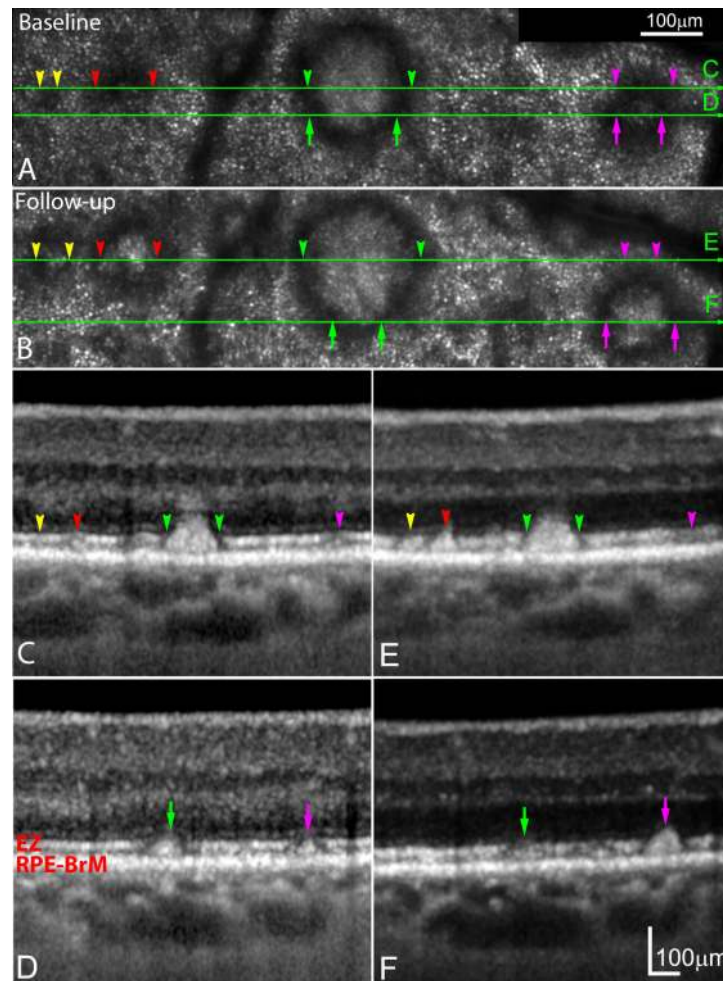


Figure 3.

Visualizing subretinal drusenoid deposits (SDD) progression by spectral domain optical coherence tomography (SD-OCT) is dependent on plane of section. **A & B.** Adaptive optics scanning laser ophthalmoscopy (AOSLO) images of the same retinal area taken at baseline and 14 months later. A stage 1 lesion (yellow arrowheads) at baseline progressed to stage 2, and a stage 2 lesion (red arrowheads) at baseline progressed to stage 3. Simultaneously, a stage 3 SDD (green arrowheads) imaged at baseline remained at the same stage and enlarged. A SDD in transition from stage 2 to stage 3 at baseline (magenta arrowheads) has fully developed to stage 3, and clearly grown above the ellipsoid zone (EZ) band. **C-D** (baseline), **E & F** (follow-up). The corresponding SD-OCT B-scans indicated by green arrow lines in (A) and (B), reveal stage-specific changes that are best appreciated in multiple scans (e.g., magenta disappears at levels C,E and grows in levels D,F). The subject (AMD-041) is a 73-year-old (at baseline) man (white non-Hispanic) with non-neovascular age-related macular degeneration (Age-Related Eye Disease Study grade 6, best-corrected visual acuity 20/25). An alternate labelling scheme not using color is available as Supplemental Digital Content 4. ELM: external limiting membrane. RPE-BrM: retinal pigment epithelium-Bruch's membrane.

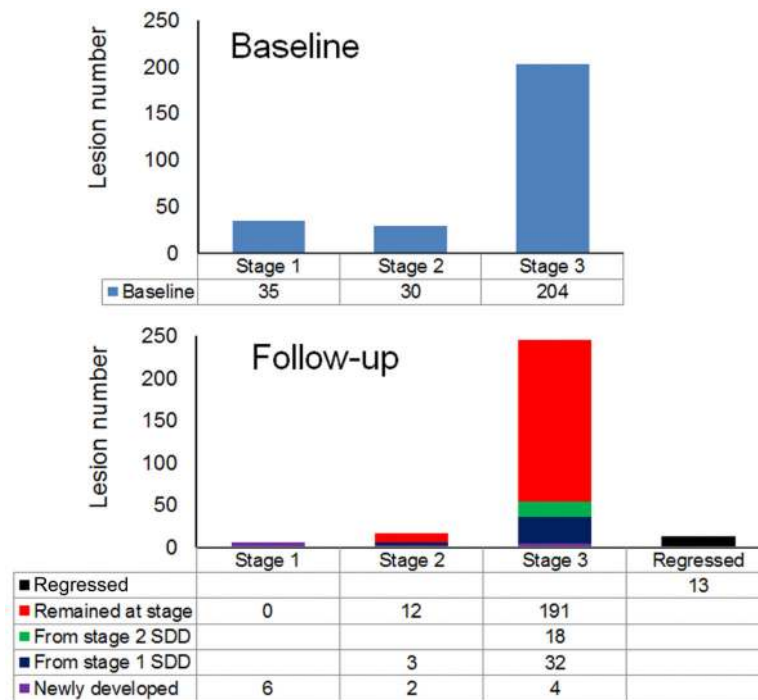


Figure 4. Transition of subretinal drusenoid deposits (SDD) between stages. A total of 269 solitary SDD were identified at baseline and at 12.25 ± 1.18 months follow-up. Lesion status at follow-up includes disappearance, transition from a less advanced stage, and de novo appearance.

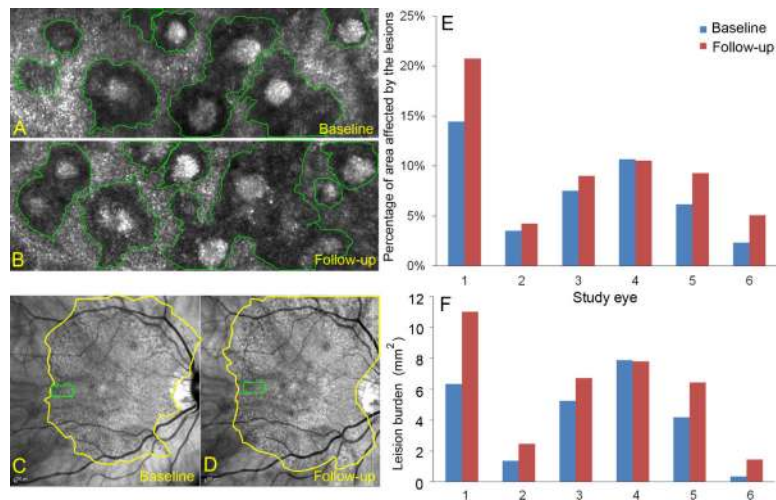


Figure 5. Quantifying the burden of subretinal drusenoid deposits (SDD) using adaptive optics scanning laser ophthalmoscopy (AOSLO) at baseline and 14-month follow-up. **A & B.** Individual SDD affected areas in regions of interest (ROI) delineated in the AOSLO, indicated by green boxes in (C) and (D). **C & D.** The entire area containing SDD in the central 30° imaged by infrared scanning laser ophthalmoscopy at baseline and 14-month follow-up. **E.** The percentage of SDD affected area in the ROI assessed by AOSLO. **F.** The burden of SDD over the area containing SDD in the central 30°, which is a product of the percentage of ROI affected by SDD and the area containing SDD in the central 30°. The eye shown in the left column (Study Eye 1) is an 84-year-old (at baseline) woman (white non-Hispanic, AMD-022) with non-neovascular age-related macular degeneration (Age-Related Eye Disease Study grade 7, best-corrected visual acuity 20/20).

TABLE 1

Equivalent diameter of areas affected by individual subretinal drusenoid deposits seen in adaptive optics scanning laser ophthalmoscopy*

Size (μm)	Stage 1		Stage 2		Stage 3	
	Baseline	Follow-up	Baseline	Follow-up	Baseline	Follow-up
Mean \pm SD [†]	51.34 \pm 18.84	66.21 \pm 23.48	61.34 \pm 25.24	76.07 \pm 19.19	90.93 \pm 27.85	100.20 \pm 26.02
Range	13.50 – 94.25	42.72 – 105.73	22.69 – 144.25	34.52 – 126.54	31.12 – 202.03	48.00 – 228.18

* Measurements include lesions that remained at stage and lesions that newly appeared at stage.

[†]SD: standard deviation.

TABLE 2

Dynamism versus net change of subretinal drusenoid deposit in 6 study eyes

Eye	New	Stable	Reabsorbed	Initial	Final	Dynamism	Abs net
1	7.81	12.91	1.51	14.42	20.72	9.32	6.30
2	0.70	3.52	0.00	3.52	4.22	0.70	0.70
3	1.86	7.16	0.34	7.50	9.02	2.20	1.52
4	1.87	8.67	2.00	10.67	10.54	3.87	-0.13
5	3.10	6.17	0.00	6.17	9.27	3.10	3.10
6	2.77	2.31	0.00	2.31	5.08	2.77	2.77
Mean						3.66	2.38
SD						2.97	2.28

Initial and final are the percentages of the region of interest (ROI) affected by subretinal drusenoid deposits (SDD) at baseline and follow-up. 'New' indicates SDD present only at baseline. 'Resorbed' indicates SDD present at baseline but not at follow-up. 'Stable' contains SDD present at both baseline and follow-up. 'Dynamism' is defined as 'new + resorbed'. 'Abs net' change is the absolute net change, or 'final - initial.' All numbers are percentage area of ROI. In some eyes, multiple ROIs were combined. SD: standard deviation.